INTERNATIONAL JOURNAL FOR NUMERICAL METHODS IN FLUIDS
Int. J. Numer. Meth. Fluids 2003; **43**:1279–1300 (DOI: 10.1002/fld.561)

Numerical simulations of non-linear wave radiation in inviscid fluid with a free surface

M. Markiewicz*,†,‡, K. Ben-Nasr and O. Mahrenholtz

Mechanik und Meerestechnik, Technische Universitaet Hamburg-Harburg, 21071 Hamburg, Germany

SUMMARY

The paper deals with the numerical simulation of non-linear wave radiation by vertical free-surface piercing structures moving horizontally in water of finite constant depth. A time-stepping approach combined with the finite element method is used to simulate the potential flows due to high-frequency oscillations of the structure. The evolution equations for the wave elevation and velocity potential at the free surface, exact up to second order, are derived using Stokes perturbation expansion. The boundary value problems up to second order at each time-step are solved using the Eulerian description and a fixed mesh of finite elements. The results of simulations are presented for vertical cylinders of circular cross section, and for sloshing waves in annular tanks. Copyright © 2003 John Wiley & Sons, Ltd.

KEY WORDS: wave radiation; free surface; non-linear waves; finite element method

1. INTRODUCTION

Steep waves and earthquakes may excite high-frequency motions of floating or gravity based offshore structures which in turn may radiate waves and thus experience additional hydrodynamic loading. If the structure motion is strong, the resulting hydrodynamic loading, which is complementary to the diffraction loading due to the seaway, is significant (see Rainey [1] and Chaplin *et al.* [2]).

While the non-linear diffraction loads have been analysed quite extensively in recent years with the use of both analytical methods (e.g. Malenica and Molin [3], Huang and Eatock Taylor [4], Newman [5], Malenica *et al.* [6]) and numerical approaches (e.g. Isaacson and Cheung [7], Kim *et al.* [8], Ferrant *et al.* [9], Ferrant and Pelletier [10]), the non-linear, high-frequency, radiation loads have received less attention [11]. However, the calculation of

*Correspondence to: M. Markiewicz, Mechanik und Meerestechnik, Technische Universität Hamburg-Harburg, 21071 Hamburg, Germany.
†E-mail: markiewicz@tu-harburg.de
‡On leave from Cracow University of Technology, Poland.

Contract/grant sponsor: Volkswagen-Stiftung; contract/grant number: 1/71 871

Received 17 October 2002
Revised 17 February 2003

the third-order, third-harmonic radiation loads on a vertical cylinder (see Markiewicz *et al.* [12]) shows that they may become significant under certain circumstances.

The work deals with the numerical simulation of non-linear wave radiation by vertical free-surface piercing structures moving horizontally in water of finite constant depth. A time-stepping approach combined with the finite element method is used for a model exact to second order to simulate the potential flow due to high-frequency oscillations of the structure.

The fully non-linear potential flow simulations of water waves usually utilize the mixed Eulerian–Lagrangian approach. The methods are based on a time-stepping procedure, in which the free-surface boundary conditions and the body boundary conditions are applied at the instantaneous free and body surfaces. The field problem is usually generated and solved by a direct BEM at each time step as both the free surface and the body move to the new positions. This simulation technique is termed as *Non-linear Numerical Wave Tank* and the review of recent developments can be found in Kim *et al.* [13] and Liu *et al.* [11].

Despite the considerable progress in this area, the implementation of the method in three dimensions is still not completely satisfactory, particularly for wave–structure interaction problems. In order to achieve a satisfactory convergence, one has to use higher-order boundary elements and regridding procedures what makes the method a very time consuming one. There are also difficulties with the behaviour of the intersection lines of a body and the free surface. The representative papers on fully non-linear 3D calculations include for instance Celebi *et al.* [14], Ferrant [15] and Liu *et al.* [11].

An interesting modification of the above mentioned method is a so-called semi-Lagrangian approach with markers on the free surface which follow not water particles but certain prescribed motion. This approach has been applied to the analysis of non-linear diffraction loads by Ferrant *et al.* [9], and to numerical simulations of sloshing waves by Wu *et al.* [16]. In the latter work, the finite elements have been used instead of boundary elements.

In the present work, three-dimensional potential flow simulations of high-frequency radiated waves have been carried out with the use of a mathematical model which is correct to second-order in the wave steepness. Similar approach has already been utilized by Isaacson and Cheung [7], Ng and Isaacson [17] and Ferrant and Pelletier [10] for diffraction and 2D radiation problems. However, to the authors' knowledge it has not been used for 3D radiation problems so far.

The numerical study of non-linear wave radiation by free-surface piercing structures undertaken in the present work has also been motivated by the phenomenon of the so-called parametrically forced wave instability. Waves generated by oscillating structures in fluid are known to become unstable when the oscillation amplitude exceeds a certain threshold value. The usual forced waves evolve into cross waves due to non-linear interaction at both the free surface and the moving structure surface (see Figure 1). This kind of instability has often been observed in laboratory water tanks (see e.g. References [18–22]) and has been analysed by many researchers (for review of earlier works see Reference [23]). It has been found that the phenomenon arises due to resonant interactions of higher-order wave components which cause the growth of a strong subharmonic cross wave. The simplified theoretical models used in the analysis so far are unable to describe satisfactorily all the observed aspects of the phenomenon. They indicate, however, that the numerical simulation must be of such an accuracy that the subtle higher-order effects will not be contaminated by numerical errors. It is believed that the numerical method for potential flow presented in the work is able to meet this requirement. Thus, it can successfully be applied in the future to the analysis of the phenomenon.

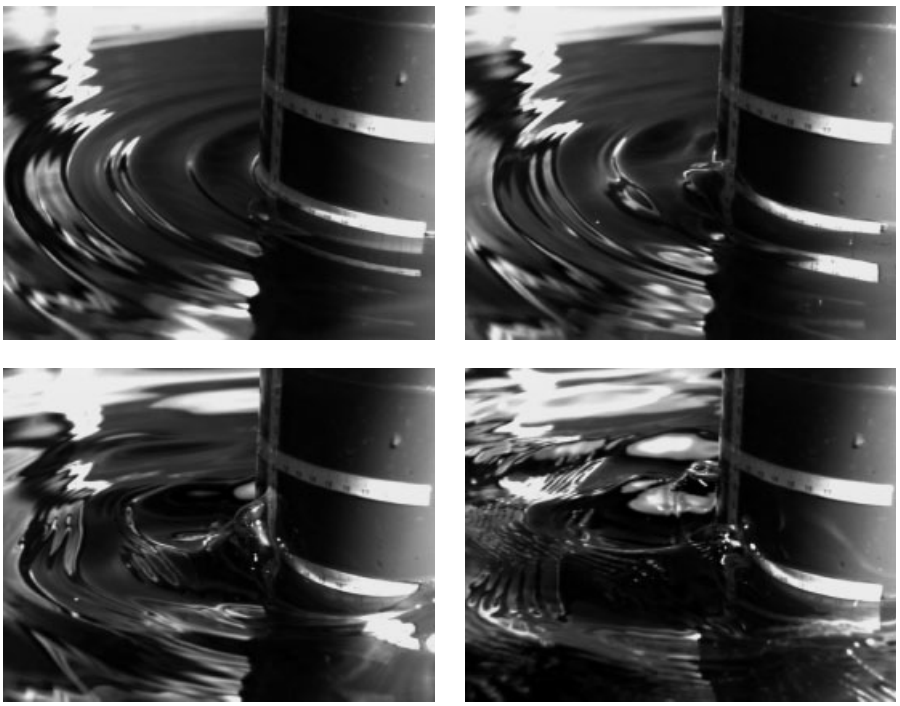

Figure 1. Evolution of waves radiated by an oscillating cylinder into a cross wave.

2. MATHEMATICAL FORMULATION

Consider the radiation of non-linear gravity waves in an inviscid fluid of constant depth h due to the forced oscillatory motion of a free-surface piercing body mounted on the bottom. The origin of a fixed co-ordinate system is located at the undisturbed free surface and the vertical z-axis is positive upward (see Figure 2).

Under the assumption that the flow is irrotational and the fluid incompressible, there exists a velocity potential $\Phi(x, y, z, t)$ which satisfies the Laplace equation in the fluid domain Ω with the following boundary conditions:

- on the free-surface $z = \eta(x, y, t)$:

$$\eta_{,t} + \nabla\eta \cdot \nabla\Phi = \Phi_{,z} \tag{1}$$

$$gz + \Phi_{,t} + \frac{1}{2}|\nabla\Phi|^2 = -P_a/\rho \tag{2}$$

- on the instantaneous body surface $z = f(x, y, t)$:

$$f_{,t} + \nabla f \cdot \nabla\Phi = \Phi_{,z} \tag{3}$$

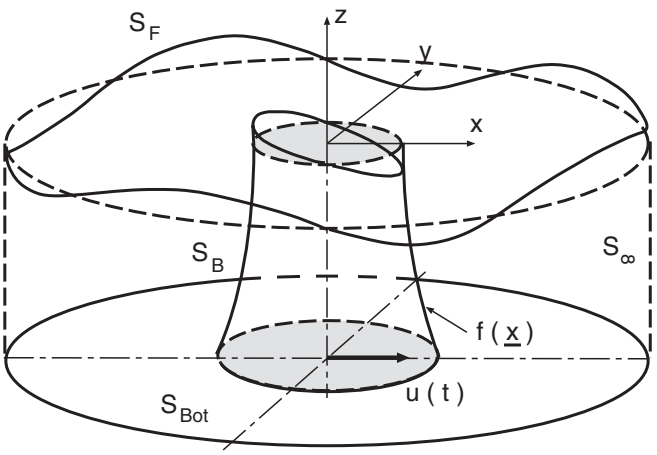

Figure 2. Definition sketch.

- on the impermeable bottom $z = -h$:

$$\Phi_{,z} = 0 \tag{4}$$

In the above formulae, subscripts after a comma denote the differentiation with respect to the proper co-ordinate, ρ is water density, g is the gravitational acceleration and P_a is the pressure on the free surface. Moreover $f(x, y, t)$ can be considered as a sum $f(x, y, t) = f_0(x, y) + \xi(x, y, t)$, where $f_0(x, y)$ describes the position of the body at rest.

The derivation of the second-order approximation to the above boundary value problem will be based on the approach used by Dommermuth and Yue [24]. According to that the free-surface potential

$$\phi(x, y, t) = \Phi(x, y, \eta(x, y, t), t) \tag{5}$$

is introduced, where the free surface is assumed to be continuous and single-valued. In terms of ϕ, the boundary conditions on the free surface are

$$\eta_{,t} = -\nabla\eta \cdot \nabla\phi + (1 + |\nabla\eta|^2)\Phi_{,z} \quad (x, y, \eta, t) \tag{6}$$

$$\phi_{,t} = -g\eta - \frac{1}{2}|\nabla\phi|^2 + \frac{1}{2}(1 + |\nabla\eta|^2)\Phi_{,z}^2(x, y, \eta, t) - P_a/\rho \tag{7}$$

The kinematic boundary condition on the instantaneous body surface

$$\xi_{,t} + \nabla(f_0 + \xi) \cdot \nabla\Phi(x, y, f) = \Phi_{,z} \quad (x, y, f) \tag{8}$$

with prescribed body motion (or deformation) $\xi = \xi(x, y, t)$, the no-flow condition

$$\Phi = 0 \tag{9}$$

on the open far-field boundary S_∞, and the initial conditions $\phi(x, y, 0)$, $\eta(x, y, 0)$ on the free-surface complete the boundary value problem considered.

Equations (6) and (7) are the evolution equations for two canonical variables η and ϕ, which can be solved numerically by a time-stepping procedure. They can be used to analyse the evolution of forced waves due to the body oscillation started from rest, and the interaction of forced waves with small disturbance waves being the result of an initial elevation. These equations have a slightly different form than those usually used in the numerical analysis (e.g. References [8, 10]). Please note, that there are no partial derivatives with respect to time on the right-hand side. Usually one has to deal with such terms like $\eta^{(1)}\partial^2\Phi^{(1)}/\partial z\,\partial t$ in which the vertical component of the particle acceleration must be approximated by a finite difference. The quality of this approximation affects the stability of numerical integration. For the present form of the evolution equations this problem does not exist.

3. NUMERICAL METHOD FOR POTENTIAL FLOW

In order to solve the non-linear wave radiation problem in potential-flow formulation, the numerical integration of the evolution equations (6) and (7) for the prescribed motion of the structure is performed. At each time step, the knowledge of vertical components of the particle velocities on the free-surface $\Phi_{,z}\ (x, y, \eta, t)$ together with gradients $\nabla\eta$ and $\nabla\phi$ is required.

For an oscillating structure, it will be assumed that its relevant characteristic length d is comparable to the wavelength λ of the radiated wave, and thus that $kd = O(1)$, k being the wave number $k = 2\pi/\lambda$. This is referred to as the *diffraction regime*. Assuming that the amplitude u_0 of the forced oscillation of the structure is small in comparison to d, i.e. $u_0/d \ll 1$, one can define $\varepsilon = ku_0 \ll 1$ as a small parameter.

In order to solve the field problem at a time step t_i, it is assumed that Φ, η and ξ are $O(\varepsilon)$ quantities. Then, the velocity potential is expressed as a perturbation series up to second order[§]

$$\Phi(x, y, z, t_i) = \sum_{m=1}^{2} \Phi^{(m)}(x, y, z, t_i) \tag{10}$$

Here and hereinafter, $(\ )^{(m)}$ denotes a quantity of $O(\varepsilon^m)$. Similar expansion is performed for $\phi(x, y, t_i)$, $\eta(x, y, t_i)$ and the prescribed motion (or deformation) of an oscillating body $\xi(x, y, t_i)$:

$$\{\phi, \eta, \xi\}(x, y, z, t_i) = \sum_{m=1}^{2} \{\phi^{(m)}, \eta^{(m)}, \xi^{(m)}\}(x, y, z, t_i) \tag{11}$$

Expanding each $\Phi^{(m)}$ evaluated on $z = \eta$ in a Taylor series about a still water level $z = 0$ one obtains

$$\phi(x, y, t_i) = \Phi(x, y, \eta, t_i) = \sum_{m=1}^{2} \sum_{k=0}^{2-m} \frac{\eta^k}{k!} \frac{\partial^k}{\partial z^k} \Phi^{(m)}(x, y, 0, t_i) \tag{12}$$

[§] The perturbation expansion could be taken up to an arbitrary order M. However, the difficulties in numerical implementation increase significantly for $m > 2$.

Similarly, one can apply to $\Phi^{(m)}$ evaluated on $z = f(x, y, t)$ a Taylor series expansion about $z = f_0(x, y)$

$$\Phi(x, y, f, t_i) = \sum_{m=1}^{2} \sum_{k=0}^{2-m} \frac{\xi^k}{k!} \frac{\partial^k}{\partial z^k} \Phi^{(m)}(x, y, f_0, t_i) \tag{13}$$

Substituting Equation (13) into boundary condition (8), one obtains

$$\xi_{,t}(x, y, t_i) + \nabla(f_0 + \xi) \cdot \nabla \left\{ \sum_{m=1}^{2} \sum_{k=0}^{2-m} \frac{\xi^k}{k!} \frac{\partial^k}{\partial z^k} \Phi^{(m)}(x, y, f_0, t_i) \right\}$$

$$= \sum_{m=1}^{2} \sum_{k=0}^{2-m} \frac{\xi^k}{k!} \frac{\partial^{k+1}}{\partial z^{k+1}} \Phi^{(m)}(x, y, f_0, t_i) \tag{14}$$

At a given instant, ϕ, η, ξ and $\xi_{,t}$ may be considered as known, being prescribed at the collocation points (x_j, y_j, z_j) on the undisturbed free surface and on the wetted surface of the body at rest $z = f_0(x, y)$. Hence, Equations (12) and (14) may be considered as the boundary conditions on a fixed fluid domain for the unknown velocity potentials $\Phi^{(m)}$.

Bearing in mind relations (11), one can collect terms at each order in Equations (12) and (14) to obtain eventually a sequence of Dirichlet boundary conditions on the undisturbed free surface $z = 0$

$$\Phi^{(m)}(x, y, 0, t_i) = \begin{cases} \phi^{(1)}(x, y, t_i) & \text{for} \quad m = 1 \\ \phi^{(2)}(x, y, t_i) - \eta^{(1)} \dfrac{\partial}{\partial z} \Phi^{(1)}(x, y, 0, t_i) & \text{for} \quad m = 2 \end{cases} \tag{15}$$

Similar procedure leads to a sequence of Neumann boundary conditions on the body surface at rest $z = f_0(x, y)$

$$\frac{\partial}{\partial z} \Phi^{(m)} - \nabla f_0 \cdot \nabla \Phi^{(m)} = \begin{cases} \dfrac{\partial \xi^{(1)}}{\partial t} & \text{for} \quad m = 1 \\ \dfrac{\partial \xi^{(2)}}{\partial t} + \nabla f_0 \cdot \nabla \left\{ \xi^{(1)} \dfrac{\partial \Phi^{(1)}}{\partial z} \right\} & \\ \quad + \nabla \xi^{(1)} \cdot \nabla \Phi^{(1)} - \xi^{(1)} \dfrac{\partial^2 \Phi^{(1)}}{\partial z^2} & \text{for} \quad m = 2 \end{cases} \tag{16}$$

Equations (15) and (16), together with Laplace equation and bottom boundary condition (4) define a sequence of linear boundary value problems for $\Phi^{(m)}$ in the domain $\Omega = \{z : -h \leqslant z \leqslant 0 \cap z \geqslant f_0(x, y)\}$. These problems ought to be solved successively at increasing order. After this has been done, the vertical velocities of free-surface particles can be computed from

$$\Phi_{,z}\ (x, y, \eta, t_i) = \sum_{m=1}^{2} \sum_{k=0}^{2-m} \frac{(\eta^{(1)} + \eta^{(2)})^k}{k!} \frac{\partial^{k+1}}{\partial z^{k+1}} \Phi^{(m)}(x, y, 0, t_i) \tag{17}$$

retaining terms up to second order.

Finally, one has to integrate numerically the following set of evolution equations:

$$\eta^{(m)}_{,t} = F^{(m)}$$

$$\phi^{(m)}_{,t} = -g\eta^{(m)} + G^{(m)} \qquad \text{for } m = 1,2 \tag{18}$$

with

$$F^{(1)} = \Phi^{(1)}_{,z}\ (x, y, 0, t)$$

$$F^{(2)} = \Phi^{(2)}_{,z}\ (x, y, 0, t) + \eta^{(1)}\Phi^{(1)}_{,zz}\ (x, y, 0, t) - \nabla\eta^{(1)} \cdot \nabla\phi^{(1)}$$

$$G^{(1)} = 0$$

$$G^{(2)} = -\frac{1}{2}\,|\nabla\phi^{(1)}|^2 + \frac{1}{2}[\Phi^{(1)}_{,z}\ (x, y, 0, t)]^2 \tag{19}$$

where the external forcing on the free surface has been neglected for the sake of simplicity (i.e. $P_a \equiv 0$).

An important advantage of this procedure is that the evolution of linear and nonlinear components of the solution can be followed separately with independent scaling of the evolution equations. This increases the accuracy of the higher-order components even for a moderate step size used in a time-marching scheme.

3.1. Finite element formulation—axisymmetric structures

The sequence of linear boundary value problems for $\Phi^{(m)}$ can be solved by using any numerical method like BEM or FEM. In this work, the finite element method is applied. The formulation of the method is given for axisymmetric structures.

In the case of an axisymmetric structure described by $z = f_0(r)$, where r is an usual radial co-ordinate defined in the plane (x, y), all the components $\Phi^{(m)}$ of the velocity potential can be expanded in a Fourier series in the circumferential direction

$$\Phi^{(m)} = \sum_{n=0}^{N} (\Phi^{(m)}_{cn}(r, z, t)\cos n\theta + \Phi^{(m)}_{sn}(r, z, t)\sin n\theta) \tag{20}$$

Similar decomposition can be applied to the components of the free-surface elevation $\eta^{(m)}$, free-surface potential $\phi^{(m)}$ and the prescribed body motion (or deformation) $\xi^{(m)}$:

$$\begin{pmatrix} \eta^{(m)} \\ \phi^{(m)} \\ \xi^{(m)} \end{pmatrix} = \sum_{n=0}^{N} \left\{ \begin{pmatrix} \eta^{(m)}_{cn}(r,t) \\ \phi^{(m)}_{cn}(r,t) \\ \xi^{(m)}_{cn}(r,t) \end{pmatrix} \cos n\theta + \begin{pmatrix} \eta^{(m)}_{sn}(r,t) \\ \phi^{(m)}_{sn}(r,t) \\ \xi^{(m)}_{sn}(r,t) \end{pmatrix} \sin n\theta \right\} \tag{21}$$

Note, that even for an axisymmetric structure its prescribed deformation or motion can generally be not axisymmetric. The initial conditions applied on the free surface can also be arbitrary. As a result, at a given order of approximation m, one obtains $2(N+1)$ independent

sets of evolution equations for the amplitudes of spatial harmonic components of $\eta^{(m)}$ and $\phi^{(m)}$:

$$\begin{aligned} \eta_{in,t}^{(m)} &= F_{in}^{(m)} \\ \phi_{in,t}^{(m)} &= -g\eta_{in}^{(m)} + G_{in}^{(m)} \end{aligned} \tag{22}$$

for $m = 1, 2,\ i = s, c,\ n = 0, 1, \ldots, N,$ with

$$\begin{aligned} F_{in}^{(1)} &= \Phi_{in,z}^{(1)}\ (r, 0, t) \\ F_{in}^{(2)} &= \Phi_{in,z}^{(2)}\ (r, 0, t) + \alpha_{in}(r, t) - \beta_{in}(r, t) \\ G_{in}^{(1)} &= 0 \\ G_{in}^{(2)} &= -\psi_{in}(r, t) + \chi_{in}(r, t) \end{aligned} \tag{23}$$

where the functions α_{in}, β_{in}, ψ_{in} and χ_{in} are given in the appendix.

The Fourier decomposition allows for a FEM formulation in two dimensions (r, z) for each spatial harmonic component $\Phi_{in}^{(m)}$ independently. The boundary value problems formulated above can be derived by using variational approach from the functional

$$J(\Phi_{in}^{(m)}) = \frac{1}{2}\int_{\Omega} (\nabla\Phi_{in}^{(m)})^2\, \mathrm{d}\Omega - \int_{S_B} V_{in}^{(m)}(s)\Phi_{in}^{(m)}\, \mathrm{d}S \tag{24}$$

where $V_{in}^{(m)}$ denotes the normal component of the velocity of the points on the wetted structure surface due to the displacement components $\xi_{in}^{(m)}$. The second integral is evaluated over the mean wetted structure surface. The free surface does not contribute to the functional since the Dirichlet (essential) boundary condition (15) is imposed on this boundary.

Calculating the variation of the functional and selecting a set of interpolation functions, one obtains a linear system of equations for the unknown values of $\Phi_{in}^{(m)}$ at nodal points

$$\mathbf{K}_n^{(m)} \cdot \Phi_{in}^{(m)} = \mathbf{R}_{in}^{(m)} \tag{25}$$

Details of this rather standard procedure are omitted here. The matrices $\mathbf{K}_n^{(m)}$ and $\mathbf{R}_{in}^{(m)}$ are given in Appendix. We note only that stiffness matrices for $\sin n\theta$ and $\cos n\theta$ components are identical and have been determined for the mesh of quadrilateral isoparametric 8-node finite elements. The mesh does not move during the time-marching procedure. Thus the global stiffness matrix for each spatial component has to be assembled and inverted only once during the computations. This reduces significantly the CPU-time and makes the method extremely efficient.

4. EXAMPLES OF COMPUTATIONS

4.1. Oscillating vertical circular cylinder

In this section, the developed solution method is applied to the radiation of water waves by a circular cylinder (radius R) mounted on the bottom in water of constant depth h. The fluid

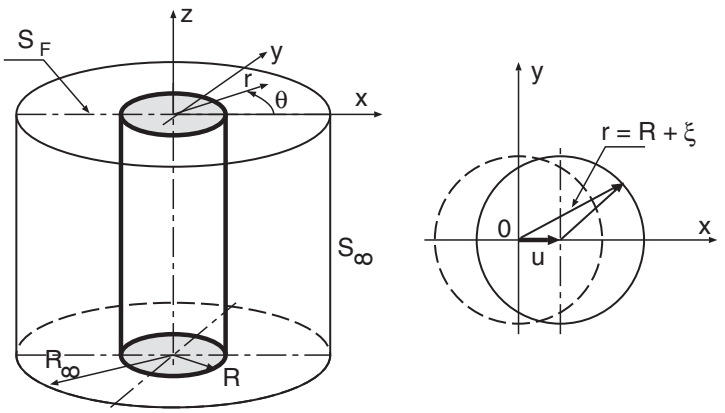

Figure 3. Cylinder configuration and the definition of the instantaneous cylinder surface.

domain is bounded by an outer circular cylinder (radius R_∞) on which the far-field boundary condition (9) is imposed (see Figure 3). The problem seems to be simple enough, however, to the authors' knowledge, its fully non-linear solution is not known so far.

The forced oscillation of the cylinder axis in the x-direction is described by the following displacement function:

$$u(t) = -u_0 \cos \Omega t \qquad \text{for } t \geqslant 0 \tag{26}$$

Assuming that $u_0 < R$, one can express the instantaneous cylinder surface (see Figure 3) in cylindrical co-ordinates as

$$r = f(\theta, t) = u(t) \cos \theta + \sqrt{R^2 - u^2(t) \sin^2 \theta} \tag{27}$$

The position of the body at rest is simply $r = R$ and $\xi(\theta, t) = f(\theta, t) - R$. Finally, the motion is assumed to start from rest with no waves on the free surface, so that the initial conditions on $z = 0$ are

$$\eta(x, y, 0) \equiv 0, \quad \phi(x, y, 0) \equiv 0 \tag{28}$$

According to the concept of the perturbation method, a power series expansion is applied to the function $\xi(\theta, t)$ describing the motion of the cylinder

$$\xi(\theta, t) = \xi^{(1)} + \xi^{(2)} + \cdots = u(t) \cos \theta - \frac{u^2(t)}{4R}(1 - \cos 2\theta) + O(u^4(t)) \tag{29}$$

where $u(t)$ has been assumed to be a first-order quantity.

In order to apply the method to this example, one has to express the boundary conditions (16) on the wetted cylinder surface $r = R$ in cylindrical co-ordinates:

$$\frac{\partial \Phi^{(m)}}{\partial r} = \begin{cases} \dfrac{\partial \xi^{(1)}}{\partial t} & \text{for } m = 1 \\ \dfrac{\partial \xi^{(2)}}{\partial t} + \dfrac{1}{R^2} \dfrac{\partial \xi^{(1)}}{\partial \theta} \dfrac{\partial \Phi^{(1)}}{\partial \theta} - \xi^{(1)} \dfrac{\partial^2 \Phi^{(1)}}{\partial r^2} & \text{for } m = 2 \end{cases} \tag{30}$$

Before starting the computations, the evolution equations are scaled by the following redefinition of the variables:

$$\Phi^{(m)} \longmapsto \frac{k^2}{\varepsilon^m \Omega}\Phi^{(m)}, \qquad \phi^{(m)} \longmapsto \frac{k^2}{\varepsilon^m \Omega}\phi^{(m)}, \qquad \eta^{(m)} \longmapsto \frac{k}{\varepsilon^m}\eta^{(m)}$$

$$\xi^{(m)} \longmapsto \frac{k}{\varepsilon^m}\xi^{(m)}, \qquad (r,z) \longmapsto k\,(r,z), \qquad t \longmapsto \Omega t$$

where k denotes the wave number of a radiated linear wave component in the far field. Moreover, a suitable modulation function

$$F(t) = \begin{cases} \dfrac{1}{2}\left[1 - \cos\dfrac{\pi t}{T_M}\right] & \text{for } t < T_M \\ 1 & \text{for } t \geqslant T_M \end{cases} \tag{31}$$

with a modulation period T_M is applied in the initial phase so that the cylinder motion in dimensionless form is described by

$$u(t) = -F(t)\cos t \tag{32}$$

The application of the function $F(t)$ allows for a smooth start of the cylinder oscillation and stabilizes numerical integration.

The numerical integration of the evolution equations is performed with the use of the implicit *Crank–Nicolson* method. The method, which is not only unconditionally stable, but it is second-order accurate in time as well as in space, has proved extremely efficient in all the computational examples discussed in the paper.

Some results for a cylinder (radius $R = 0.09$ m, water depth $h = 0.42$ m) oscillating at the frequency 1.7 Hz with the amplitude $u_0 = 0.018$ m are shown in Figures 4–10. A corresponding wave number and wave length in far field are $k = 11.1$ 1/m, $\lambda = 0.565$ m. The amplitude of the cylinder motion has been selected to produce a rather steep wave with $\varepsilon = 0.2$. The radius of the outer cylinder was chosen as $R_\infty = 5.74$ m so that the water area in the radial direction is equal to 10λ. A vertical section of the fluid domain was discretized by 30080 eight-node rectangular elements.

Figure 4 shows the time history of the second-order axisymmetric component of the free-surface elevation at two nodes. A solid line represents the node located on the cylinder at $r = R$, a dashed line represents the node at $r = R + \lambda/4$. One can observe a stable steady state reached after approximately five periods of the cylinder oscillations. Note that the oscillation frequency of this component is twice as the cylinder frequency. The other components reveal the same stable behaviour.

As already mentioned, the present method allows for an independent study of the evolution of all wave components present in the solution. In our example, due to a specific excitation (see Equation (29)), only one linear ($\cos\theta$) and two non-linear (axisymmetric and $\cos 2\theta$) components are present in the solution which is exact up to second order. The instantaneous free-surface elevation (dimensionless) for each of these components after 10 periods of cylinder oscillations is shown in Figures 5, 6 and 7.

The total non-linear free-surface elevation is obtained by assembling the properly scaled ($\varepsilon = 0.2$) linear and non-linear components (see Figure 8). The non-linear effects concentrate

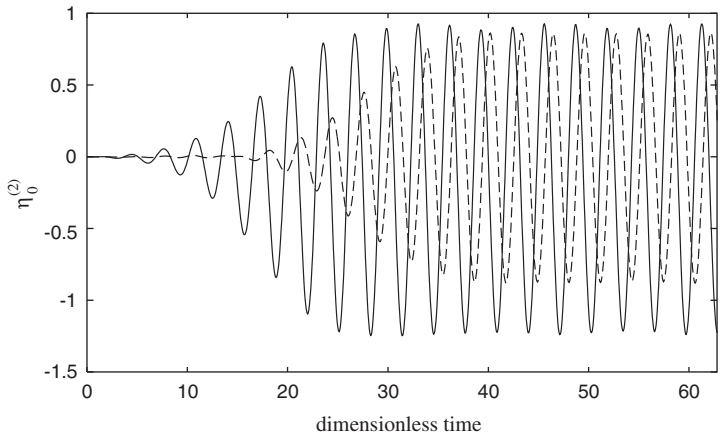

Figure 4. Evolution of the wave $\eta_0^{(2)}$ at $r = R$ (solid line), and at $r = R + \lambda/4$ (dashed line).

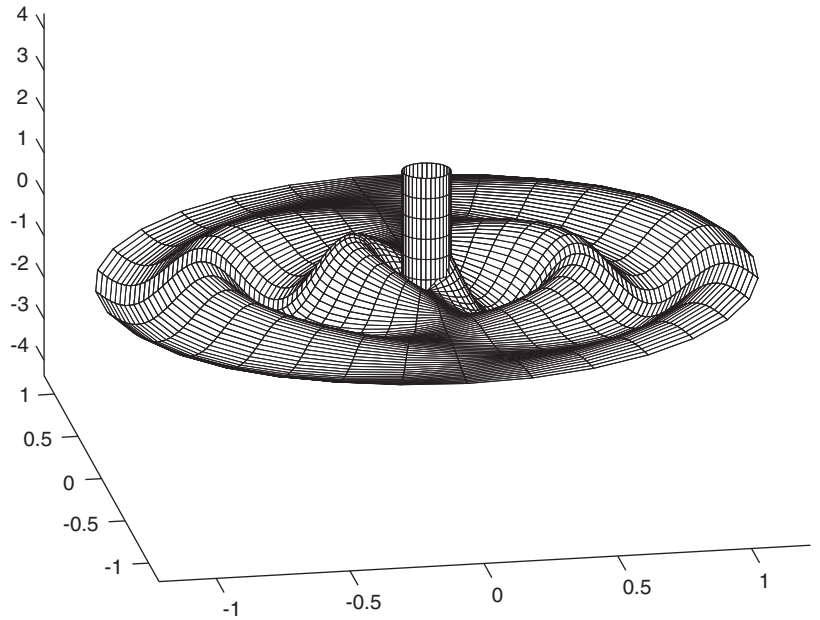

Figure 5. Instantaneous free surface elevation after 10 periods, linear component.

in the vicinity of the oscillating cylinder and decay quite fast, as shown in Figures 9 and 10. The numerical approach confirms the result well known from the analysis in frequency domain (see Markiewicz *et al.* [12]) that the non-linear radiated wave field must consist of so-called *locked* and *free* components, both are clearly visible in Figure 10. The former with the length approximately equal to $\lambda/2$, with λ being the wavelength of the linear component in far field, emerges due to nonlinear interaction of the first order components on the free surface.

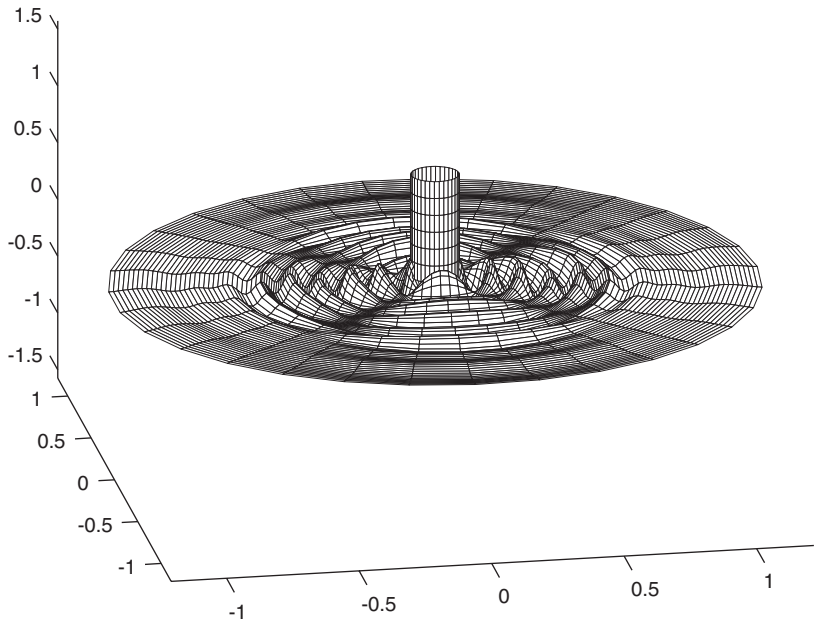

Figure 6. $\cos(2\theta)$-component of the free surface after 10 periods.

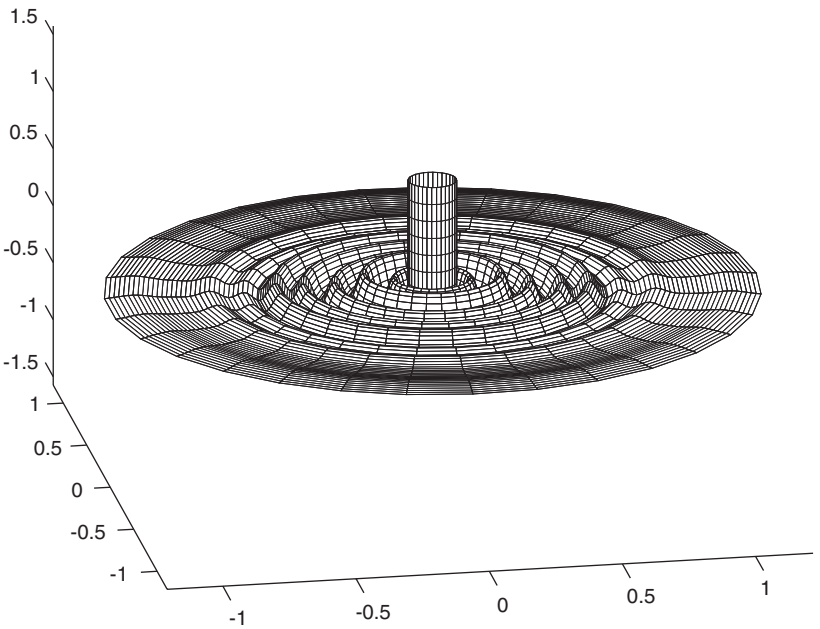

Figure 7. Axisymmetric component of the free surface after 10 periods.

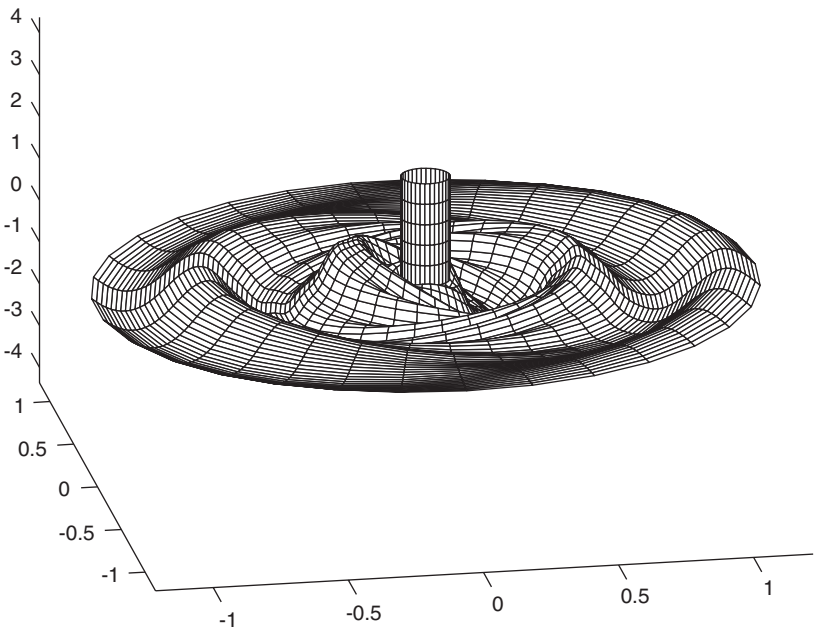

Figure 8. Instantaneous free-surface elevation after 10 periods, linear and non-linear components.

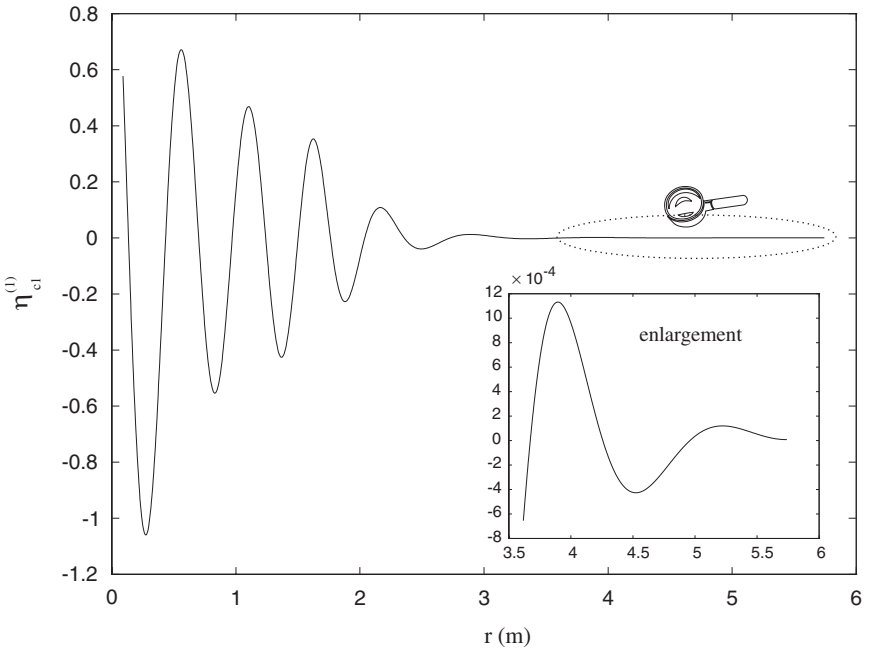

Figure 9. Wave contour at $\theta = 0^\circ$ after 10 periods for the linear component.

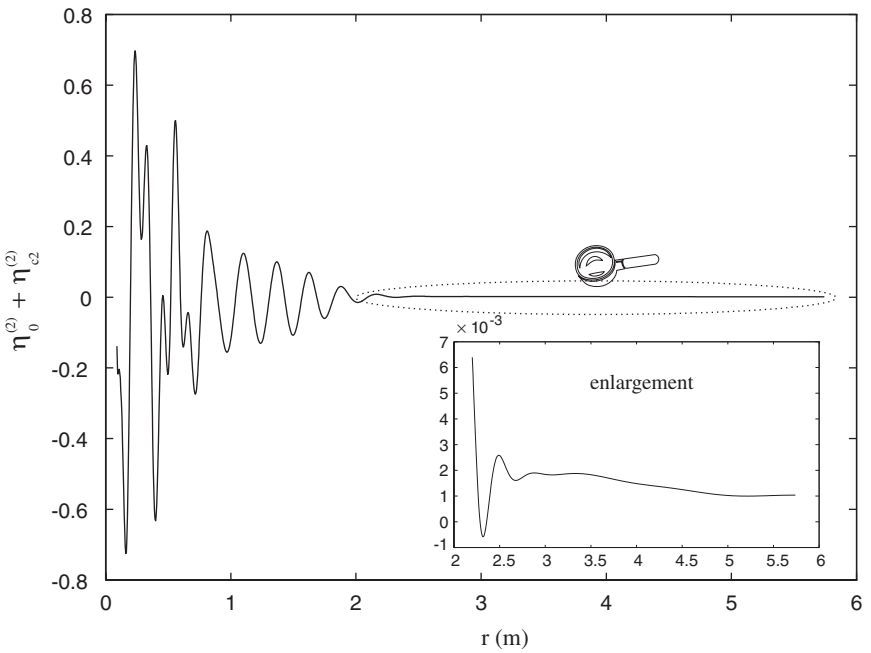

Figure 10. Wave contour at $\theta = 0^\circ$ after 10 periods for the non-linear components.

The latter has its length approximately equal to $\lambda/4$ and is directly forced by a wavemaker (cylinder). The *locked* component propagates with the same phase speed as the linear one $c = \Omega/k$, whereas the phase speed of the *free* component is equal to $c = \Omega/2k$. Moreover, Figure 10 shows that the *locked* component associated with the wave number $2k$ decays slower than the *free* component associated with the wave number $4k$. The analysis in the frequency domain leads to a similar conclusion.

It is apparent that the parameter ε affects only the final result i.e. the assembling of the solution. Thus, having performed the simulation for one magnitude of the cylinder oscillation one is able to construct the solution for any magnitude. Certainly, the weakness of this approach is that for large values of the wave steepness ε the solution obtained has nothing to do with a real wave field, particularly, one is unable to model breaking of waves. Nevertheless, for waves of moderate steepness the method yields correct results, which can be confirmed by comparison with experiments. Here, we only refer to the first picture shown in Figure 1 where a rather steep cylindrical wave is shown. One can observe the non-linear components 'riding' on a linear one.

4.2. *Sloshing waves in an annular tank*

In this example sloshing of fluid in a tank built of two coaxial vertical cylinders is investigated. The parameters of the tank are: $R_{\text{in}} = 0.09\,\text{m}$, $R_{\text{out}} = 1.09\,\text{m}$, water depth $h = 0.75\,\text{m}$. The waves are induced by a prescribed free-surface potential at $t = 0$. More specifically, the dimensionless

initial conditions are:

$$\eta(r,\theta,0)\equiv 0, \qquad \phi(r,\theta,0)=\phi_{c1}^{(1)}\cos\theta+\phi_{s1}^{(1)}\sin\theta \tag{33}$$

with

$$\phi_{c1}^{(1)}=\phi_{s1}^{(1)}=1.5\cdot[J_1(k_2r)+\beta_2 Y_1(k_2r)], \qquad \beta_2=-\frac{J_1'(k_2R_{\text{in}})}{Y_1'(k_2R_{\text{in}})} \tag{34}$$

The Bessel functions J_1 and Y_1 are computed for the value $k_2=4.7605$, which is the second eigenvalue of a linear sloshing problem in such an annular tank i.e. k_2 is the second root of the characteristic equation

$$J_1'(kR_{\text{in}})Y_1'(kR_{\text{out}})-J_1'(kR_{\text{out}})Y_1'(kR_{\text{in}})=0 \tag{35}$$

Thus, the initial conditions (33) describe the second eigenmode of a linear sloshing problem. The parameters correspond to the initial wave steepness $\varepsilon=0.2$.

The fluid domain was discretized in one vertical section by 6336 equally spaced eight-node elements, 96 horizontally and 66 vertically. The aim of the calculation was to observe the development of non-linear wave components which should inevitably emerge during sloshing since the initial wave satisfies only a linearized free-surface condition. One would also expect that the linear wave component, as a second eigenmode, will be preserved during simulations

Some results of the simulations are shown in Figures 11–16. The evolution of the free surface in the initial phase is shown within a half of a sloshing period in Figure 11. After five further sloshing periods, the non-linear components on the free surface become more pronounced (see Figure 12). The same effects can also be observed on the snapshots of the free surface at some instants (see Figures 13 and 14). One can observe that the non-linear components appear first at the inner cylinder (due to large gradients in circumferential direction), then propagate towards the outer cylinder.

The initial conditions of the sloshing have been chosen in such a form (33), (34) which allows for an easy check of the accuracy of computations.

Consider the evolution equations for the second-order components $\eta_{c2}^{(2)}$, $\phi_{c2}^{(2)}$. Using Equations (22), (23), the relations given in the appendix, and noting that only the first-harmonic components $(\sin\theta,\cos\theta)$ are present in the linear wave, one obtains

$$\begin{aligned}
\eta_{c2,t}^{(2)} &= \Phi_{c2,z}^{(2)}+\frac{1}{2}\left\{\eta_{c1}^{(1)}\Phi_{c1,zz}^{(1)}-\eta_{s1}^{(1)}\Phi_{s1,zz}^{(1)}+\eta_{s1,r}^{(1)}\phi_{s1,r}^{(1)}-\eta_{c1,r}^{(1)}\phi_{c1,r}^{(1)}\right.\\
&\quad\left.+\frac{1}{r^2}(\eta_{c1}^{(1)}\phi_{c1}^{(1)}-\eta_{s1}^{(1)}\phi_{s1}^{(1)})\right\}\\
\phi_{c2,t}^{(2)} &= -g\eta_{c2}^{(2)}+\frac{1}{4}\left\{\phi_{s1,r}^{(1)2}-\phi_{c1,r}^{(1)2}+\Phi_{c1,z}^{(1)2}-\Phi_{s1,z}^{(1)2}+\frac{1}{r^2}(\phi_{c1}^{(1)2}-\phi_{s1}^{(1)2})\right\}
\end{aligned} \tag{36}$$

By virtue of (33) and (34) $\phi_{c1}^{(1)}(r,t)$ is equal to $\phi_{s1}^{(1)}(r,t)$ and consequently $\eta_{c1}^{(1)}(r,t)\equiv\eta_{s1}^{(1)}(r,t)$. Since the nonlinear components are assumed to be zero at $t=0$, it follows from (15) and (36) that $\phi_{c2}^{(2)}(t)$ and $\eta_{c2}^{(2)}(t)$ are identically equal to zero on the whole free surface in this case. Thus, the time history of $\eta_{c2}^{(2)}$ can be treated as a measure of computational error. The

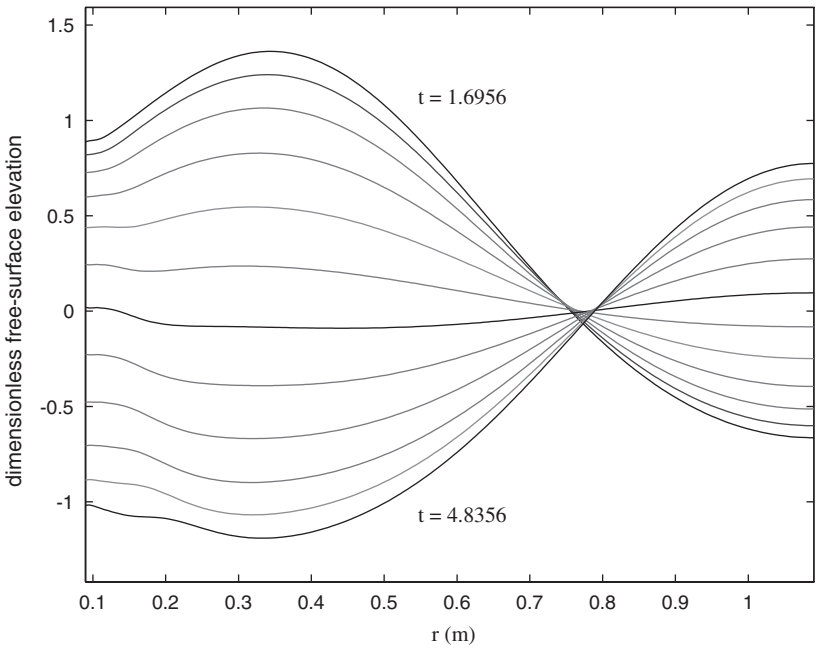

Figure 11. Wave elevations at $\theta = 45^\circ$ in the initial phase of sloshing between $t = 1.6956$ and 4.8356, equidistant distribution within a half of a sloshing period.

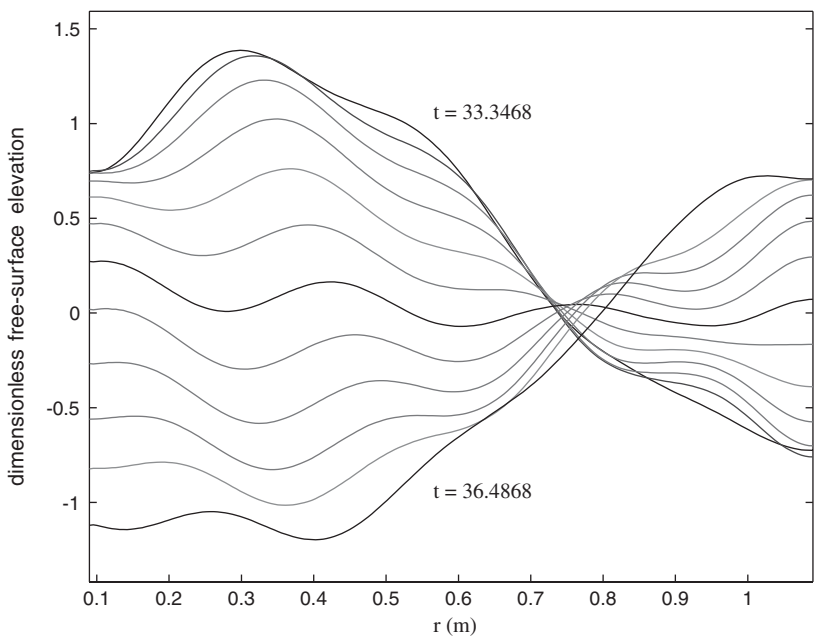

Figure 12. Wave elevations at $\theta = 45^\circ$ after five sloshing periods between $t = 33.3468$ and 36.4868, equidistant distribution within a half of a sloshing period.

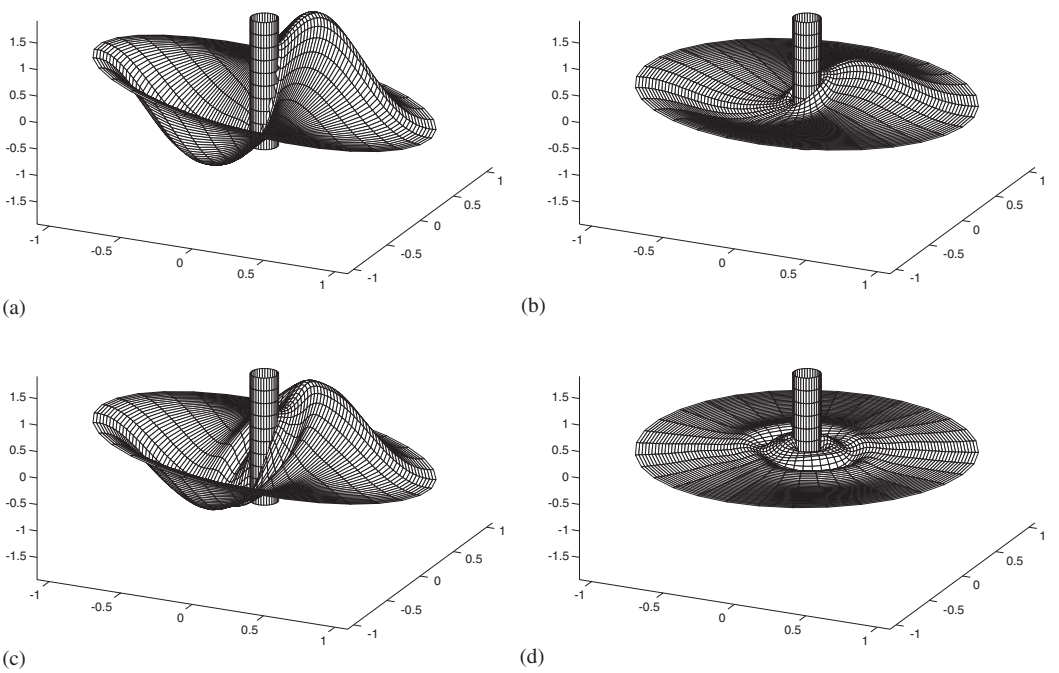

Figure 13. Sloshing waves at $t = 1.70$ (a), $t = 2.89$ (b) $t = 7.98$ (c) and $t = 9.55$ (d).

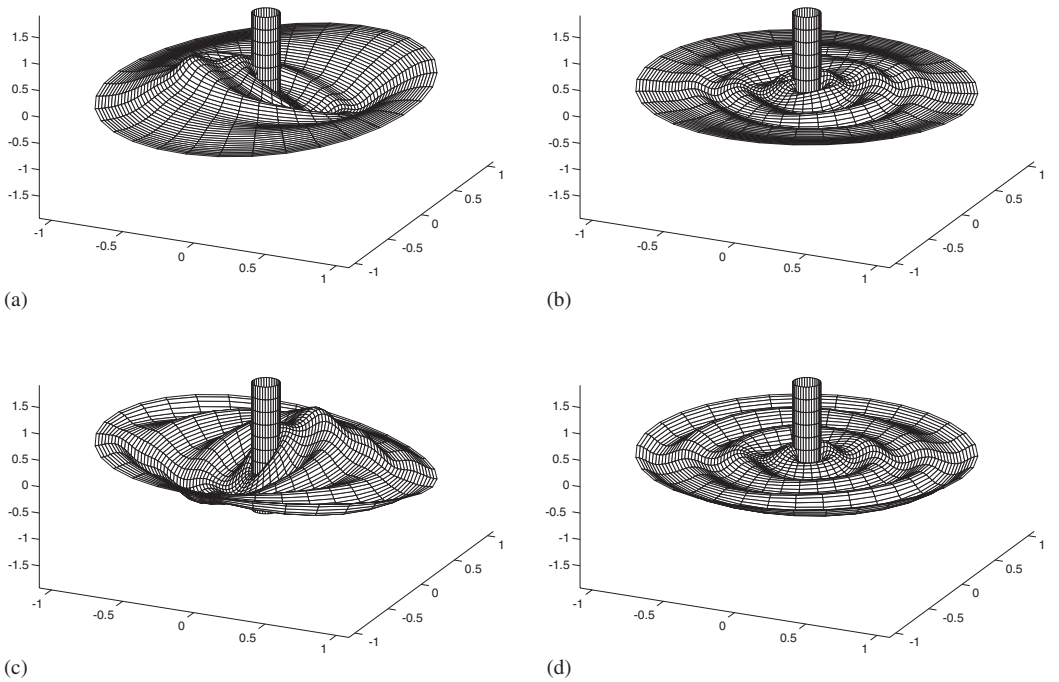

Figure 14. Sloshing waves at $t = 16.40$ (a), $t = 19.2$ (b) $t = 34.5$ (c) and $t = 35.0$ (d).

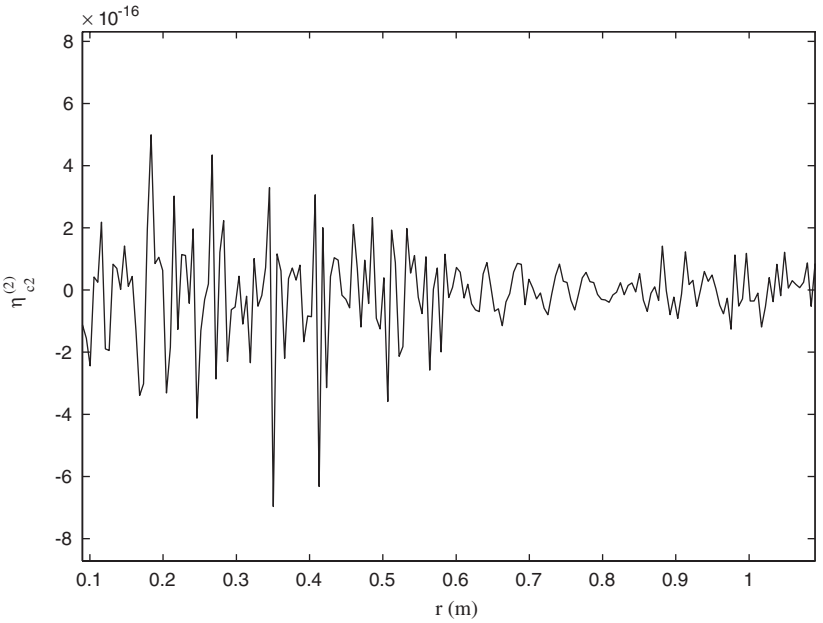

Figure 15. Elevation of $\eta_{c2}^{(2)}$ at $\theta = 0^\circ$ after 12 sloshing periods.

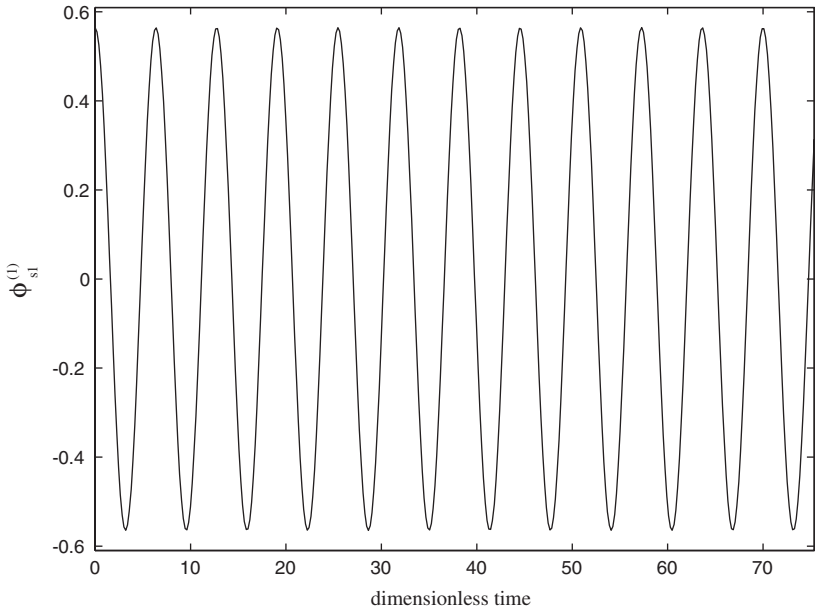

Figure 16. Time history of the $\phi_{s1}^{(1)}$ component of the free-surface potential at $r = R_{in}$, $\theta = 0^\circ$.

elevation of $\eta_{c2}^{(2)}$ after twelve sloshing periods shown in Figure 15 indicates a clear numerical zero. On the other hand, Figure 16 shows that the linear wave component remains preserved during sloshing. Both figures confirm a very high accuracy of the method.

5. CONCLUSIONS

A new numerical method has been developed for the simulation of non-linear waves radiated by oscillating structures or produced by an initial disturbance of the free surface. The method, which is correct to second order in wave steepness, has proved extremely efficient when applied both to the radiation and sloshing of waves. The evolution equations for each order of approximation have been scaled independently. It enables one to study the linear and non-linear effects separately.

The finite element approach used in the numerical procedure proved to be effective. The sequence of boundary value problems for all wave components is solved on a fixed domain, thus the matrix of the equation system has to be assembled and decomposed only once during simulations. Corner points can be treated in a standard way. Generally, the method applies to generation of waves of a moderate steepness, for which the free surface is a single-valued function. At the present stage of development, the axisymmetric wave generators subjected to (not necessarily) periodic oscillation or wave propagation in cylindrical tanks can be considered.

In the numerical example referring to the radiation problem, the far-field boundary condition (Equation (9)) has been taken in an extremely simple form stating that the disturbance will not reach the outer boundary during simulations. This implies a large outer radius of the disretized domain or a limited simulation time since Equation (9) will result in spurious wave reflections when radiated waves reach the outer boundary. Certainly, one could apply instead more sophisticated radiation conditions or use damping zones at the open far-field boundaries as in [10]. Such extensions can easily be included in the formulation of the method. However, the method is such computationally inexpensive that we decided to use the simplest form of the far-field boundary condition in our numerical tests.

The method presented in the work is still not capable to deal with the parametric wave instability mentioned in the Introduction. In order to account for such phenomena, it has to be generalized to include third-order effects. A theoretical part of this task has already been completed. Currently, the extensive work is going on the numerical implementation of the procedure.

The method is based on perturbation expansion and thus it cannot be extended to account for fully non-linear wave simulations including wave breaking. Any extension beyond the third order seems to be infeasible. However, its efficiency and accuracy in modelling of second- and hopefully third-order effects makes it attractive to an offshore engineer.

APPENDIX A

Functions α_{in}, β_{in}, ψ_{in} *and* χ_{in}:

In order to determine the functions α_{in}, β_{in}, ψ_{in} and χ_{in} which appear in the functions $F^{(2)}$ and $G^{(2)}$, Equation (23), the following trigonometric identities are needed:

$$\sum_{n=0}^{\infty} a_n \cos n\theta \sum_{m=0}^{\infty} b_m \cos m\theta = \frac{1}{2} \sum_{n=0}^{\infty} \left\{ \varepsilon_n \sum_{m=0}^{\infty} (a_m b_{m+n} + a_{m+n} b_m) + \sum_{m=0}^{n} a_{n-m} b_m \right\} \cos n\theta$$

$$\sum_{n=0}^{\infty} a_n \sin n\theta \sum_{m=0}^{\infty} b_m \sin m\theta = \frac{1}{2} \sum_{n=0}^{\infty} \left\{ \varepsilon_n \sum_{m=0}^{\infty} (a_m b_{m+n} + a_{m+n} b_m) - \sum_{m=0}^{n} a_{n-m} b_m \right\} \cos n\theta$$

$$\sum_{n=0}^{\infty} a_n \sin n\theta \sum_{m=0}^{\infty} b_m \cos m\theta = \frac{1}{2} \sum_{n=1}^{\infty} \left\{ \sum_{m=0}^{\infty} (a_m b_{m+n} - a_{m+n} b_m) + \sum_{m=0}^{n} a_{n-m} b_m \right\} \sin n\theta$$

$$\sum_{n=0}^{\infty} n a_n \cos n\theta \sum_{m=0}^{\infty} m b_m \cos m\theta = \frac{1}{2} \sum_{n=0}^{\infty} \left\{ \varepsilon_n \sum_{m=0}^{\infty} m(m+n)(a_m b_{m+n} + a_{m+n} b_m) + \sum_{m=0}^{n} m(n-m) a_{n-m} b_m \right\} \cos n\theta$$

$$\sum_{n=0}^{\infty} n a_n \sin n\theta \sum_{m=0}^{\infty} m b_m \sin m\theta = \frac{1}{2} \sum_{n=0}^{\infty} \left\{ \varepsilon_n \sum_{m=0}^{\infty} m(m+n)(a_m b_{m+n} + a_{m+n} b_m) - \sum_{m=0}^{n} m(n-m) a_{n-m} b_m \right\} \cos n\theta$$

$$\sum_{n=0}^{\infty} n a_n \sin n\theta \sum_{m=0}^{\infty} m b_m \cos m\theta = \frac{1}{2} \sum_{n=1}^{\infty} \left\{ \sum_{m=0}^{\infty} m(m+n)(a_m b_{m+n} - a_{m+n} b_m) + \sum_{m=0}^{n} m(n-m) a_{n-m} b_m \right\} \sin n\theta$$

with $\varepsilon_0 = \frac{1}{2}$ and $\varepsilon_n = 1$ for $n \geqslant 1$.

Applying these identities to the products of first-order quantities in Equations (19) one obtains

$$\alpha_{cn}(r,t) = \frac{1}{2} \varepsilon_n \sum_{m=0}^{\infty} (\eta^{(1)}_{cm} \Phi^{(1)}_{c(m+n),zz} + \eta^{(1)}_{c(m+n)} \Phi^{(1)}_{cm,zz} + \eta^{(1)}_{sm} \Phi^{(1)}_{s(m+n),zz} + \eta^{(1)}_{s(m+n)} \Phi^{(1)}_{sm,zz}) + \frac{1}{2} \sum_{m=0}^{n} (\eta^{(1)}_{c(n-m)} \Phi^{(1)}_{cm,zz} - \eta^{(1)}_{s(n-m)} \Phi^{(1)}_{sm,zz}) \quad \text{for } z = 0$$

$$\alpha_{sn}(r,t) = \frac{1}{2} \sum_{m=0}^{\infty} (\eta^{(1)}_{s(m+n)} \Phi^{(1)}_{cm,zz} + \eta^{(1)}_{cm} \Phi^{(1)}_{s(m+n),zz} - \eta^{(1)}_{sm} \Phi^{(1)}_{c(m+n),zz} - \eta^{(1)}_{c(m+n)} \Phi^{(1)}_{sm,zz}) + \frac{1}{2} \sum_{m=0}^{n} (\eta^{(1)}_{sm} \Phi^{(1)}_{c(n-m),zz} + \eta^{(1)}_{c(n-m)} \Phi^{(1)}_{sm,zz}) \quad \text{for } z = 0$$

$$\beta_{cn}(r,t)=\frac{1}{2}\,\varepsilon_n\sum_{m=0}^{\infty}\Big\{\eta^{(1)}_{cm,r}\phi^{(1)}_{c(m+n),r}+\eta^{(1)}_{c(m+n),r}\phi^{(1)}_{cm,r}+\eta^{(1)}_{sm,r}\phi^{(1)}_{s(m+n),r}+\eta^{(1)}_{s(m+n),r}\phi^{(1)}_{sm,r}$$
$$+\ \frac{m(m+n)}{r^2}(\eta^{(1)}_{cm}\phi^{(1)}_{c(m+n)}+\eta^{(1)}_{c(m+n)}\phi^{(1)}_{cm}+\eta^{(1)}_{sm}\phi^{(1)}_{s(m+n)}+\eta^{(1)}_{s(m+n)}\phi^{(1)}_{sm})\Big\}$$
$$+\frac{1}{2}\sum_{m=0}^{n}\Big\{\eta^{(1)}_{c(n-m),r}\phi^{(1)}_{cm,r}-\eta^{(1)}_{s(n-m),r}\phi^{(1)}_{sm,r}+\frac{m(n-m)}{r^2}(\eta^{(1)}_{s(n-m)}\phi^{(1)}_{sm}-\eta^{(1)}_{c(n-m)}\phi^{(1)}_{cm})\Big\}$$

$$\beta_{sn}(r,t)=\frac{1}{2}\sum_{m=0}^{\infty}\Big\{\eta^{(1)}_{cm,r}\phi^{(1)}_{s(m+n),r}+\eta^{(1)}_{s(m+n),r}\phi^{(1)}_{cm,r}-\eta^{(1)}_{sm,r}\phi^{(1)}_{c(m+n),r}-\eta^{(1)}_{c(m+n),r}\phi^{(1)}_{sm,r}$$
$$-\ \frac{m(m+n)}{r^2}(\eta^{(1)}_{cm}\phi^{(1)}_{s(m+n)}+\eta^{(1)}_{s(m+n)}\phi^{(1)}_{cm}-\eta^{(1)}_{sm}\phi^{(1)}_{c(m+n)}-\eta^{(1)}_{c(m+n)}\phi^{(1)}_{sm})\Big\}$$
$$+\frac{1}{2}\sum_{m=0}^{n}\Big\{\eta^{(1)}_{c(n-m),r}\phi^{(1)}_{sm,r}+\eta^{(1)}_{sm,r}\phi^{(1)}_{c(n-m),r}-\frac{m(n-m)}{r^2}(\eta^{(1)}_{s(n-m)}\phi^{(1)}_{cm}+\eta^{(1)}_{cm}\phi^{(1)}_{s(n-m)})\Big\}$$

$$\psi_{cn}(r,t)=\frac{1}{2}\,\varepsilon_n\sum_{m=0}^{\infty}\Big\{\phi^{(1)}_{cm,r}\phi^{(1)}_{c(m+n),r}+\phi^{(1)}_{sm,r}\phi^{(1)}_{s(m+n),r}+\frac{m(m+n)}{r^2}(\phi^{(1)}_{cm}\phi^{(1)}_{c(m+n)}+\phi^{(1)}_{sm}\phi^{(1)}_{s(m+n)})\Big\}$$
$$+\frac{1}{4}\sum_{m=0}^{n}\Big\{\phi^{(1)}_{c(n-m),r}\phi^{(1)}_{cm,r}-\phi^{(1)}_{s(n-m),r}\phi^{(1)}_{sm,r}+\frac{m(n-m)}{r^2}(\phi^{(1)}_{s(n-m)}\phi^{(1)}_{sm}-\phi^{(1)}_{c(n-m)}\phi^{(1)}_{cm})\Big\}$$

$$\psi_{sn}(r,t)=\frac{1}{2}\sum_{m=0}^{\infty}\Big\{\phi^{(1)}_{cm,r}\phi^{(1)}_{s(m+n),r}-\phi^{(1)}_{sm,r}\phi^{(1)}_{c(m+n),r}-\frac{m(m+n)}{r^2}(\phi^{(1)}_{cm}\phi^{(1)}_{s(m+n)}-\phi^{(1)}_{sm}\phi^{(1)}_{c(m+n)})\Big\}$$
$$+\frac{1}{2}\sum_{m=0}^{n}\left(\phi^{(1)}_{c(n-m),r}\phi^{(1)}_{sm,r}-\frac{m(n-m)}{r^2}\,\phi^{(1)}_{cm}\phi^{(1)}_{s(n-m)}\right)$$

$$\chi_{cn}(r,t)=\frac{1}{2}\,\varepsilon_n\sum_{m=0}^{\infty}(\Phi^{(1)}_{cm,z}\Phi^{(1)}_{c(m+n),z}+\Phi^{(1)}_{sm,z}\Phi^{(1)}_{s(m+n),z})+\frac{1}{4}\sum_{m=0}^{n}(\Phi^{(1)}_{c(n-m),z}\Phi^{(1)}_{cm,z}-\Phi^{(1)}_{s(n-m),z}\Phi^{(1)}_{sm,z})$$

$$\chi_{sn}(r,t)=\frac{1}{2}\sum_{m=0}^{\infty}(\Phi^{(1)}_{cm,z}\Phi^{(1)}_{s(m+n),z}-\Phi^{(1)}_{sm,z}\Phi^{(1)}_{c(m+n),z})+\frac{1}{2}\sum_{m=0}^{n}\Phi^{(1)}_{c(n-m),z}\Phi^{(1)}_{sm,z}\quad\text{for}\quad z=0\qquad\text{(A1)}$$

Matrices $\mathbf{K}_n^{(m)}$ and $\mathbf{R}_{\text{in}}^{(m)}$ *of the finite element equations*:
The global stiffness matrix $\mathbf{K}_n^{(m)}$ and right-hand side vector $\mathbf{R}_{\text{in}}^{(m)}$ are assembled from the element matrices

$$\{\mathbf{K}_n^{(m)}\}^e_{jk}=\int_{\Omega^e}\nabla N_j\nabla N_k\,\mathrm{d}\Omega^e+n^2\int_{\Omega^e}\frac{1}{r^2}\,N_jN_k\,\mathrm{d}\Omega^e$$
$$\{\mathbf{R}_{\text{in}}^{(m)}\}^e_j=\int_{S_B^e}V_{\text{in}}^{(m)}N_j\,\mathrm{d}S^e$$

with the quadratic interpolation functions N_j of the serendipity family.

ACKNOWLEDGEMENTS

The work was accomplished within a co-operation project between the Technical University Hamburg-Harburg and Cracow University of Technology. The financial support was provided by the Volkswagen Foundation. The authors gratefully acknowledge this support.

REFERENCES

1. Rainey RCT. Violent surface motion around vertical cylinders in large steep waves—is it the result of the step change in relative acceleration. In *Proceedings of 12th International Workshop on Water Waves and Floating Bodies.* Carrey-le-Rouet: France, 1997.
2. Chaplin JR, Retzler CH, Rainey RCT. Waves generated by a vertical cylinder moving in still waves. *Proceedings of 14th International Workshop on Water Waves and Floating Bodies*, Japan, 1999.
3. Malenica Š, Molin B. Third-harmonic wave diffraction by a vertical cylinder. *Journal of Fluid Mechanics* 1995; **302**:203–229.
4. Huang JB, Eatock Taylor R. Semi-analytical solution for second-order wave diffraction by a truncated circular cylinder in monochromatic waves. *Journal of Fluid Mechanics* 1996; **319**:171–196.
5. Newman JN. Second-order wave force on a vertical cylinder. *Journal of Fluid Mechanics* 1996; **320**:417–443.
6. Malenica Š, Eatock Taylor R, Huang R. Second-order water wave diffraction by an array of vertical cylinders. *Journal of Fluid Mechanics* 1999; **390**:249–373.
7. Isaacson M, Cheung KF. Time domain second order wave diffraction in three dimensions. *Journal of Waterways, Port, Coastal & Ocean Engineering* 1992; **118**:496–516.
8. Kim Y, Kring DC. Sclavounos PD. Time-domain solution of second order wave diffraction. *Applied Ocean Research* 1997; **19**:235–249.
9. Ferrant P, Malenica Š, Molin B. Nonlinear wave loads and runup on a vertical cylinder. In *Nonlinear Water Wave Interaction*, Mahrenholtz O, Markiewicz M (eds). WIT Press: Southampton, 1999; 101–135.
10. Ferrant P, Pelletier K. Second order wave diffraction patterns about complex offshore structures. *Proceedings of the 10th International Offshore and Polar Engineering Conference*, Seattle, Vol III USA, May 28–June 2, 2000; 686–693.
11. Liu Y, Xue M, Yue DKP. Computation of fully non-linear three-dimensional wave-wave and wave-body interactions. Part 2. Nonlinear waves and forces on a body. *Journal of Fluid Mechanics* 2001; **438**:41–66.
12. Markiewicz M, Łetkowski P, Mahrenholtz O. Third-order hydrodynamic loads on an oscillating vertical cylinder in water. *Journal of Offshore Mechanics and Arctic Engineering* 1999; **121**:16–21.
13. Kim CH, Clement A, Tanizawa K. Recent research and development of numerical wave tank—a review. *International Journal of Offshore and Polar Engineering* 1999; **9**(4):241–256.
14. Celebi MS, Kim MH, Beck RF. Fully non-linear 3D wave tank simulation. *Journal of Ship Research* 1998; **42**(1):33–45.
15. Ferrant P. Non-linear interactions of long-crested wave packets with a three-dimensional body. *Proceedings of the 22nd ONR Symposium on Naval Hydrodynamics*, Washington, USA, 1998: 403–415.
16. Wu GX, Ma QW, Eatock Taylor R. Numerical simulation of sloshing waves in a 3D tank based on a finite element method. *Applied Ocean Research* 1998; **20**:337–355.
17. Ng JY, Isaacson M. Second-order wave interaction with two-dimensional floating bodies by a time-domain method. *Applied Ocean Research* 1993; **15**:95–105.
18. Schuler M. Der Umschlag von Oberflächenwellen. *Zeitschrift für Angewandte Mathematik und Mechanik* 1933; **13**:443–446.
19. Barnard BJS, Pritchard WG. Cross-waves, Part 2 Experiments. *Journal of Fluid Mechanics* 1972; **55**:245–255.
20. Lichter S, Bernoff AJ. Stability of steady cross-waves: theory and experiments. *Physical Review* 1988; **A37**: 1663–1667.
21. Taneda S. Visual observations of the flow around a half-submerged oscillating sphere. *Journal of Fluid Mechanics* 1991; **227**:492–209.
22. Markiewicz M, Mahrenholtz O. Instability of water waves in three-dimensional radiation problems. In *Nonlinear Water Wave Interaction*, Mahrenholtz O, Markiewicz M (eds). WIT Press: Southampton, 1999; 199–252.
23. Markiewicz M, Mahrenholtz O. Progressive cross waves due to the horizontal oscillations of a vertical cylinder in water. Evolution equations. *Journal of Engineering Mathematics* 1998; **34**:227–247.
24. Dommermuth GG, Yue DKP. A high-order spectral method for the study of nonlinear gravity waves. *Journal of Fluid Mechanics* 1987; **184**:267–288.

